Space Vector Based Investigation of Overmodulation Region of Inverter Fed Multiphase AC Drives

Péter Stumpf, Kristóf Bándy
Dept. of Automation and Applied Informatics
Budapest University of Technology and Economics
stumpf@aut.bme.hu
bandyk@edu.bme.hu

Sándor Halász
Dept. of Electric Power Engineering
Budapest University of Technology and Economics
halasz.sandor@vet.bme.hu

***Abstract*—Space vector investigation of multi-phase inverters in overmodulation region is presented in the paper to study ac motor harmonic losses. It is shown that, in full overmodulation region the optimization of additional switching angles of inverter does not ensure the acceptable decrease of motor harmonic losses. Therefore the motor voltage region above 80-87% of the inverter maximum possible value is virtually restricted at least for a steady state operation. At the same time, the space vector investigation of multi-phase system - in comparison to other methods of investigation and opposite to 3-phase system is more difficult and seems less effective.**

***Index Terms*—Multi-phase drive, Voltage source inverter, AC machine**

I. Introduction

The structure of *m*-phase inverter-fed ac drive is presented in Fig. 1. In this case the phase number of motor and inverter is bigger than 3. Advantages of multi-phase inverter-motor system, like better fault tolerance (it can operate even during phase open fault), lower motor torque ripples, smaller power rating of converter semiconductors and lower phase current for a given voltage rating, have been well evidenced in the past years [1]–[5]. These properties made multiphase machine suitable for special applications, like using them in electric cars.

Pulse Width Modulation (PWM) control of multi-phase inverters has become a research hotspot in multi-phase motor application. Similarly to three-phase system, most commonly Space Vector Modulation or Sinusoidal Modulation are used to control mutliphase drives. A detailed overview and comparison about PWM control methods of multiphase drives can be found in [3]–[5]. Analytic calculation of voltage harmonics is presented for multiphase inverters with an odd number of phases in paper [6]. Paper [7] introduces a multifrequency modulation technique for dual three-phase voltage source converters supplying six-phase drives.

Overmodulation region control of multi-phase inverters requires much more attention than in the three-phase case, because effective impedances differ between fundamental and some specific harmonics components not involved within the mechanical energy conversion. These low-order harmonic voltage components face very low effective impedances in the multiphase drive, increasing the harmonic Joule losses in the machine [8].

Research supported by the National Research, Development and Innovation Office (NKFIH) under the grant FK 124913. The research reported in this paper was supported by the BME NC TKP2020 grant of NKFIH Hungary.

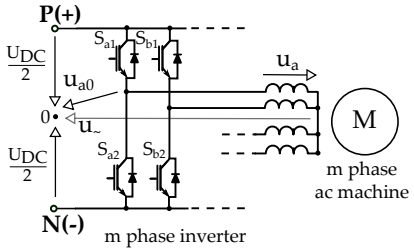

Fig. 1. Structure of multi-phase inverter-fed ac drive

The overmodulation region of multi-phase inverter-fed ac drives is investigated in [9], [11] by computation of phase and line voltages of multi-phase system. This paper uses space (Park) vector method for study harmonic losses of multiphase drives in the overmodulation region. As it will be shown later, drawing vector paths gives a very important information on magnitude of stator and rotor harmonic losses and show which harmonic order produce those losses.

II. State of the Art

In multi-phase system the number of possible phase-end connections to dc bars are equal to 2^m. If m is a prime number there are only two zero voltage vectors while the other $2^m - 2$ voltage vectors produce $(2^m - 2)/(2m)$ vector systems. In each system there are $2m$ vectors with phase shift between two neighboring vectors π/m . Thus, for example for $m = 7$ the number of possible space vectors is equal to 128. Two from these are zero vectors while the others create $126/14 = 9$ different vector systems. Each system consists of 14 vectors with phase shift $\pi/7$ between two neighboring ones. If m is not a prime number there will be more than two zero vectors.

In Table I those 9 vectors are presented (related to $U_{DC}/2$, where U_{DC} is the dc link voltage of the inverter) whose direction is close to the positive a phase direction. It can be seen that seven vectors have direction of phase a and only two vectors have a small phase shift regarding the axis of phase a.

For m-phase system the space vector investigation requires the use of a different number of coordinate systems. For

TABLE I
SPACE VECTORS IN POSITIVE DIRECTION OF PHASE a IN FIG.2a, $m = 7$

Phase Connection		Vector	Vector/$(U_{DC}/2)$
P (+DC)	N(-DC)		
a,b,g	c,d,e,f	$\frac{4+8cos(2\pi/7)}{7}$	1.284
a,b,c,f,g	d,e	$8cos(\pi/7)/7$	1.03
b,g	a,c,d,e,f	$8cos(2\pi/7)/7$	0.713
a	b,c,d,e,f,g	4/7	0.571
b,c,f,g	a,d,e	$\frac{4-8cos(\pi/7)}{7}$	0.458
a,c,f	b,d,e,g	$\frac{4-8cos(3\pi/7)}{7}$	0.317
a,b,d,e,g	c,f	$8cos(3\pi/7)/7$	0.254
a,b,f	c,d,e,g	$4\sqrt{2}/7$	$0.808e^{j0.137}$
a,c,g	b,d,e,f	$4\sqrt{2}/7$	$0.808e^{-j0.137}$

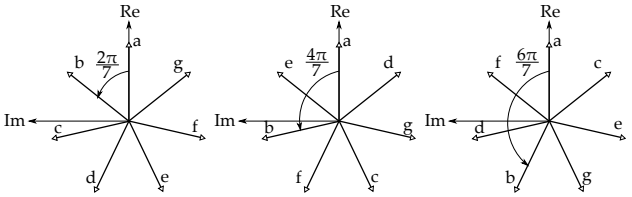

(a) Phase shift $\frac{2\pi}{7}$ (b) Phase shift $\frac{4\pi}{7}$ (c) Phase shift $\frac{6\pi}{7}$

Fig. 2. Coordinate systems for $m = 7$

example for $m = 4$ or 5 one must use two coordinate systems while for $m = 6$ or 7 there will be three ones etc. [4], [5], [10]. For the latter case, the coordinate systems are given in Fig. 2. It can be seen that, the coordinate systems differ by sequence of phases. Further on the 7-phase system is investigated since this one is not yet over complicated and at the same time shows all difficulties of multi-phase space vector method application.

According to the definition the space vectors for $m = 7$ are:

$$\mathbf{U}_I = \frac{2}{7}\Big(u_a + u_b\mathbf{a} + u_c\mathbf{a}^2 + u_d\mathbf{a}^3 + u_e\mathbf{a}^4 + u_f\mathbf{a}^5 + u_g\mathbf{a}^6\Big);$$

$$\begin{aligned}\mathbf{U}_{II} =& \frac{2}{7}\Big(u_a + u_b\mathbf{a}^2 + u_c\mathbf{a}^4 + u_d\mathbf{a}^6 + u_e\mathbf{a}^8 + u_f\mathbf{a}^{10} \\ &+ u_g\mathbf{a}^{12}\Big); \\ \mathbf{U}_{III} =& \frac{2}{7}\Big(u_a + u_b\mathbf{a}^3 + u_c\mathbf{a}^6 + u_d\mathbf{a}^9 + u_e\mathbf{a}^{12} \\ &+ u_f\mathbf{a}^{15} + u_g\mathbf{a}^{18}\Big),\end{aligned} \quad (1)$$

where u_a, u_b ... u_g are the phase voltages, $\mathbf{U}_I$,$\mathbf{U}_{II}$ and $\mathbf{U}_{III}$ are the voltage space vectors of the first, second and third coordinate systems in Fig. 2 and $a = e^{j2\pi/7}$. The $\mathbf{U}_I$ vector contains voltage harmonics of order $1 \pm 14k$. The $\mathbf{U}_{II}$ vector components are voltage harmonics of order $-5 - 14k$ and $9 + 14k$ while in $\mathbf{U}_{III}$ there are harmonics of order $3 + 14k$ and $-11 - 14k$, where $k = 0, 1, 2, 3....$ It should be noted only harmonics of order $1 \pm 14k$ produce rotor currents and motor torque.

III. OVERMODULATION

In case of three phase system the overmodulation region is $0.907 \leq \hat{U}_1/\hat{U}_{1,max} \leq 1$, where $\hat{U}_1$ the motor peak fundamental votlage and $\hat{U}_{1,max} = \frac{2U_{DC}}{\pi}$ is the maximum possible value of this fundamental voltage.

Motor harmonic losses can be characterized by the loss factor, which is the square of rms value of the stator harmonic flux as follows

$$\Delta\Psi^2 = \sum_{\nu>1}^{\infty}\left(\frac{U_\nu}{U_1\nu}\right)^2, \quad (2)$$

where U_ν is the rms value of the voltage harmonic order of ν.

It is assumed that in per unit system the motor rated voltage is equal to the maximal inverter voltage $\hat{U}_{1,max} = \frac{2U_{DC}}{\pi}$, and the rated frequency f_{1r} corresponds to $\hat{U}_{1,max}$ voltage.

In six-step operation mode of a three-phase inverter the value of loss factor is $\Delta\Psi^2 = 0.00215$. It is more useful to characterize the motor harmonic losses by a relative loss-factor which is the relation of $\Delta\Psi^2$ to 0.00215:

$$k_\Psi = \Delta\Psi^2/0.00215. \quad (3)$$

In the case of $k_\Psi = 1$ approximately 15% motor power degradation is necessary, while for $k_\Psi \leq 0.1$ the motor power degradation is usually unnecessary.

For a multi-phase system ($m > 3$) the maximum possible value of a motor fundamental voltage is the same as for three phase system. In case of even number of phases the motor star point voltage in any time is zero thus the phase voltage and the motor phase end voltage to the $'0'$ middle point of DC link voltage (see Fig. 1) are the same. Therefore, for any even number of phases the overmodulation region - for $m > 7$ - begins from $\hat{U}_1 = U_{DC}/2 = \pi\hat{U}_{1,max}/4 = 0.785\hat{U}_{1,max} = 0.785$ pu. With odd m the overmodulation region of multi-phase inverters begins at $\hat{U}_1 = \frac{U_{DC}}{2}\frac{1}{\cos(\pi/(2m))}$. Therefore, the overmodulation region of multi-phase inverters virtually begins at $\hat{U}_1 = U_{DC}/2 = 0.785$ pu and only for $m = 5$ it is possible to increase the normal region up to still sensible value of $\hat{U}_1 = 0.823$ pu.

IV. SPACE VECTORS FOR FULL CONTROL

For $\hat{U}_{1,max}$ (full control) the switching number, denoted later on by γ, of one transistor is $\gamma = 1$. For this case the stator flux space vector paths are presented in Fig. 3. In Fig. 3(a) the space vector path of the first flux component is given in stationary coordinate system. The stator flux vector path gives 14-side polygonal of 14 voltage vectors with amplitude $1.284U_{DC}/2$.

From Fig. 3(a) it is clear that, with appropriate PWM control assuming an infinitely high switching frequency, the $1 \pm 14k$ low order harmonics can be eliminated if the fundamental voltage is less than radius of the circle internal to 14-angle polygon as

$$\hat{U}_1 \leq 1.284cos(\pi/14)(\pi/4) = 0.9832\,\text{pu} \quad (4)$$

Thus the above constraint of the linear control region is determined by low order harmonics of II and III coordinate systems.

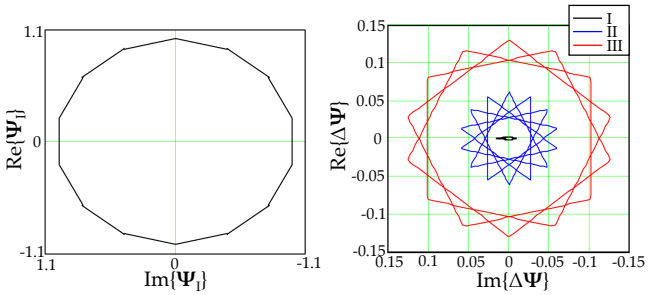

(a) Flux vector path of I coordinate system (b) Harmonic flux vector paths of coordinate systems I, II and III

Fig. 3. Full inverter control, $\gamma = 1$

In Fig. 3(b) the space vector components are drawn in three different coordinate systems. The used space vectors for all three coordinate systems are given in Table II. In the first coordinate system the flux vector path is drawn in synchronously rotated coordinate system and only the harmonic flux is shown. It can be seen that this flux harmonic component is very small therefore the square of rotor harmonic current in case of $m = 7$ will be very small too.

In the second and third coordinate system the flux vector paths are given in their own stationary coordinate system. These fluxes do not contain the fundamental component. It can be seen that, the rms value of these fluxes are very high. Therefore, the stator harmonic current has considerable value which is mainly determined by a third order current harmonic (III coordinate system) and by a fifth order current harmonic (II coordinate system). Therefore at $\hat{U}_{1,max}$ the loss-factor of multi-phase inverters is more than 6 times higher than for $m = 3$. In case of $m = 7$ the total loss-factor and its components in the first, second and third coordinate system will be

$$\begin{aligned}\Delta\Psi^2 =& \Delta\Psi_I^2 + \Delta\Psi_{II}^2 + \Delta\Psi_{III}^2 = \\ =& 0.00006 + 0.00177 + 0.0124 = 0.0143. \end{aligned} \quad (5)$$

Assuming a transient reactance $L' = 0.12$ pu and stator leakage reactance $L_\sigma = 0.1$ pu, the square of harmonic current is

$$\begin{aligned}\Delta i^2 =& \frac{\Delta\Psi_I^2}{L'^2} + \frac{\Delta\Psi_{II}^2 + \Delta\Psi_{III}^2}{L_\sigma^2} = \\ =& \frac{0.00006}{0.12^2} + \frac{0.014173}{0.1^2} = 1.42. \end{aligned} \quad (6)$$

With this low value of L' the rotor skin effect is taken into account. At the same time the rotor current is very small

$$\Delta i_r^2 = \frac{\Delta\Psi_I^2}{L'^2}\frac{0.00006}{0.12^2} = 0.0042. \quad (7)$$

It should be noted that L' depends on the rotor frequency. However, low order rotor current harmonics in overmodulation region, assuming standard 50 Hz stator frequency, have frequency over 120-150 Hz therefore the skin effect decreases the rotor leakage reactance considerably. Therefore, assuming L' to be constant is a fairly good approximation.

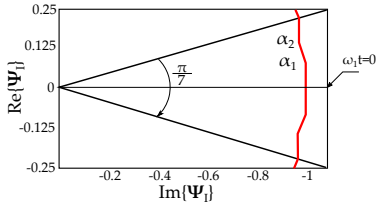

(a) Flux vector path of 1. coordinate system, $\hat{U}_1 = 0.985$

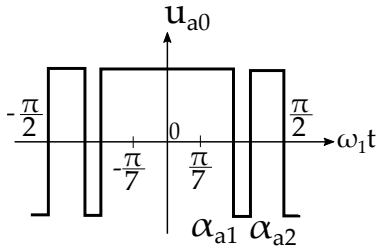

(b) Phase end voltage u_{a0}

Fig. 4. Additional switching, $\gamma = 5$

Thus, the stator current harmonics produce higher losses than the rated current, while the rotor current losses are very low. Mainly it is explained by the existence of third order stator current harmonic because the third order voltage harmonic has the amplitude $\hat{U}_3 = \hat{U}_{1,max}/3$. However, this current harmonic produce zero stator magnetomotive force (mmf) value in the air gap of machine so it cannot produce rotor current.

V. Additional Switching

The unacceptable value on harmonic losses can be lowered by inverter voltage control with additional switchings. For a different motor fundamental voltage the additional switching angles α_i (see Fig. 4) are determined by Newton-Rapson method for the smallest value of loss-factor. The method of calculation for three-phase system is introduced in [11]. Due to the symmetry of vector paths computations were performed only for the $-\pi/14 \leq \omega_1 t \leq \pi/14$ region. The space vector paths in the figures are drawn by knowing all possible voltage vectors. These vectors depend on the magnitude of the reference voltage and they are gathered in Table II. The voltage and flux harmonic vectors are calculated for all coordinate systems. The vector paths are obtained by summation of harmonic flux vectors up $\nu = 10000$.

The calculated α_{a1} and α_{a2} switching angles for $\gamma = 5$ as the function of $\hat{U}_1$ between 0.8 and 1 is plotted on Fig. 5(a). The value of k_Ψ relative loss-factor for different phase numbers for $\gamma = 5$ is shown in Fig. 5(b). As it can be seen by decreasing the fundamental voltage by 2-3% e.g., the relative loss-factor of three-phase system can be diminished to $k_{\Psi,3} = 0.17 - 0.22$ pu. Nevertheless, for $m > 3$ the relative loss-factor of this voltage region cannot be lowered to an acceptable value. Figure 5(c) presents the value of loss factors in different coordinate systems for $m = 7$ and $\gamma = 5$.

From Fig. 4 it is seen that, the switching in time α_1 and α_2 happens in phase c and in time $-\alpha_1$ and $-\alpha_2$ in phase f ($-\pi/14 \leq \omega t \leq \pi/14$). From Fig. 4 it is clear that $\alpha_1 = \alpha_{c1} = \alpha_{a1} - 3\pi/7$ and $\alpha_2 = \alpha_{c2} = \alpha_{a2} - 3\pi/7$.

TABLE II
VOLTAGE SPACE VECTORS BETWEEN $0 \leq \omega_1 t \leq \pi/14$, $\pi/4 \leq \hat{U}_1 \leq 1$

$\hat{U}_1$ [pu]	Angles [rad]	Phase connection		Vector		
		+DC	-DC	Fig.2a	Fig.2b	Fig.2c
1	$\alpha_1 = \alpha_2 = 0$	a,b,g	c,d,e,f	1.284	0.317	-0.458
$0.968 < \hat{U}_1 \leq 1$	$\alpha_{c2} > \alpha_{c1} > 0$	a,b,g	c,d,e,f	1.284	0.317	0.458
		a,b,c,g	d,e,f	$1.284e^{\pi/7}$	$-0.317e^{2\pi/7}$	$-0.458e^{3\pi/7}$
		a,b,g	c,d,e,f	1.284	0.317	-0.458
$0.939 < \hat{U}_1 \leq 0.968$	$\alpha_{c2} > \alpha_{f1} \geq 0$	a,b,c,f,g	d,e	1.03	-0.713	0.254
		a,b,c,g	d,e,f	$1.284e^{\pi/7}$	$-0.317e^{2\pi/7}$	$-0.458e^{3\pi/7}$
		a,b,g	c,d,e,f	1.284	0.317	-0.458
$0.884 < \hat{U}_1 \leq 0.939$	$\alpha_{f1} > \alpha_{c2} \geq 0$	a,b,c,f,g	d,e	1.03	-0.713	0.254
		a,b,f,g	c,d,e	$1.284e^{-\pi/7}$	$-0.317e^{2\pi/7}$	$-0.458e^{3\pi/7}$
		a,b,g	c,d,e,f	1.284	0.317	-0.458
$0.877 < \hat{U}_1 \leq 0.884$	$\alpha_{f1} > \alpha_{f2} \geq 0$	a,b,g	c,d,e,f	1.284	0.317	-0.458
		a,b,f,g	c,d,e	$1.284e^{-\pi/7}$	$-0.317e^{-2\pi/7}$	$-0.458e^{-3\pi/7}$
	$\lvert\alpha_{f1}\rvert \leq \pi/14$	a,b,g	c,d,e,f	1.284	0.317	-0.458
$0.857 < \hat{U}_1 \leq 0.877$	$\alpha_1 = \alpha_{g2}$	a,b,g	c,d,e,f	1.284	0.317	-0.458
		a,b	c,d,e,f,g	$1.03e^{\pi/7}$	$-0.713e^{2\pi/7}$	$0.254e^{3\pi/7}$
	$\alpha_2 = \pi/7 + \alpha_{f2}$	a,b,f	c,d,e,g	$0.808e^{0.137}$	$0.808e^{1.658}$	$0.808e^{1.035}$
$0.807 < \hat{U}_1 \leq 0.857$	$\alpha_1 = \alpha_{g1}$	a,b,g	c,d,e,f	1.284	0.317	-0.458
		a,b	c,d,e,f,g	$1.03e^{\pi/7}$	$0.713e^{2\pi/7}$	$0.254e^{3\pi/7}$
	$\alpha_2 = \alpha_{g2}$	a,b,g	c,d,e,f	1.284	0.317	-0.458
$\pi/4 < \hat{U}_1 \leq 0.807$	$\alpha_1 = 4\pi/7 - \alpha_{b1}$	a	b,c,d,e,f,g	0.571	0.571	0.571
		a,b	c,d,e,f,g	$1.03e^{\pi/7}$	$0.713e^{2\pi/7}$	$0.254e^{3\pi/7}$
	$\alpha_2 = \alpha_{g1}$	a,b,g	c,d,e,f	1.284	0.317	-0.458

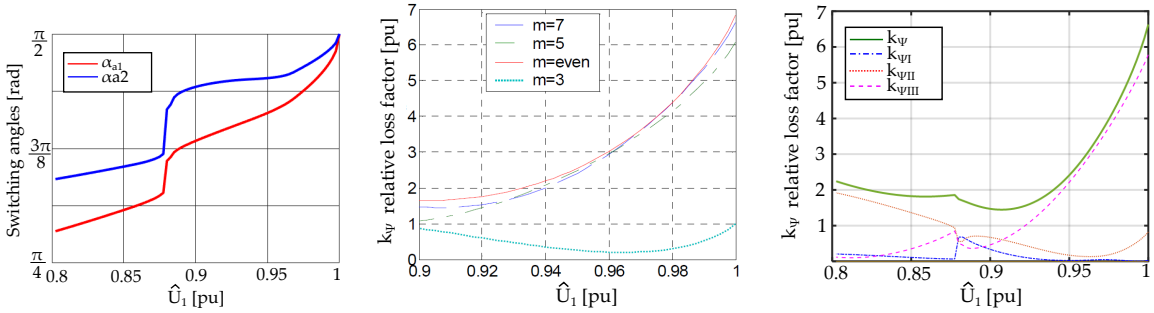

(a) Calculated switching angles, $m = 7$, $\gamma = 5$,

(b) k_Ψ relative loss-factor for different phase numbers, $\gamma = 5$

(c) Value of k_Ψ relative loss-factor in different coordinate systems, $m = 7$, $\gamma = 5$

Fig. 5. Calculated switching angles and the value of k_Ψ relative loss-factor, $\gamma = 5$

The additional switching decreases the motor fundamental voltage and considerably diminishes the motor harmonic loss. From Table I it can be seen that, there are several different voltage regions in which the space vectors of the system are different. These voltage regions are drawn in Fig. 6.

For $\hat{U}_1 = 0.985$ the flux vector path in the first coordinate system is presented in Fig. 7. In Fig. 7 all the flux vector paths are given similarly to Fig. 3. In this case the lossfactors are

$$\begin{aligned}\Delta\Psi^2 =& \Delta\Psi_I^2 + \Delta\Psi_{II}^2 + \Delta\Psi_{III}^2 = \\ =& 0.000056 + 0.000619 + 0.00962 = 0.0104. \end{aligned} \quad (8)$$

It should be noted that in (2) the loss-factors are given by assuming that the motor voltage is proportional to the speed. Hence, the motor fundamental flux is equal to the rated one. In comparison with (6) the loss-factors of the second and third components decrease (to 40% and to 77%, respectively), while the first component decreases only by 6%.

The results of computation for $\hat{U}_1 = 0.95$ pu are presented in Fig. 8. Only the first vectors of all the three coordinate systems differ from the previous case. The shape of flux path in the first coordinate system is very similar (see Fig. 8(c) and Fig. 3(a)). All the three flux paths are given in Fig. 8(c). It can be seen that, the loss factor $\Delta\Psi_I^2$ scarcely decreases

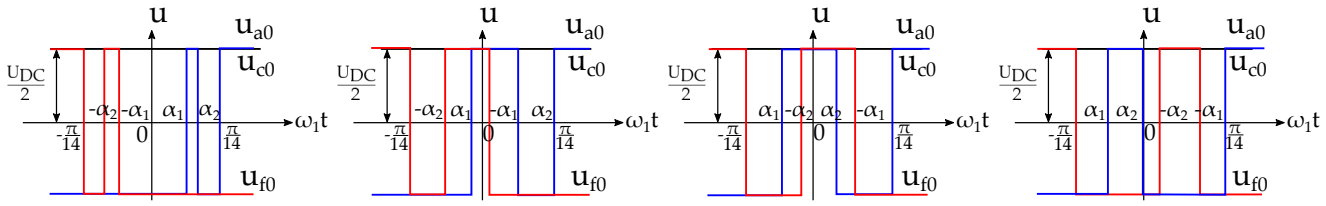

(a) $0.968 < \hat{U}_1 \leq 1$ (b) $0.939 < \hat{U}_1 \leq 0.968$ (c) $0.884 < \hat{U}_1 \leq 0.939$ (d) $0.877 < \hat{U}_1 \leq 0.884$

Fig. 6. Switching position for different voltage regions, $-\pi/14 \leq \omega_1 t \leq \pi/14$

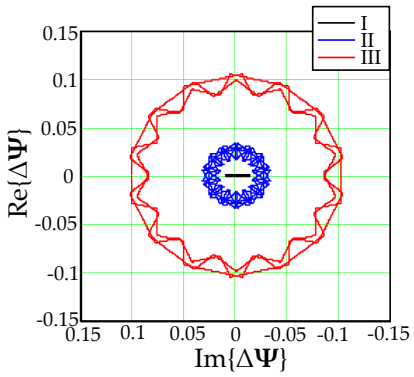

Fig. 7. Harmonic flux vector paths of coordinate systems I, II and III, $\gamma = 5$, $U_1 = 0.985$ pu

while $\Delta\Psi^2_{II} = 0.00035$ and $\Delta\Psi^2_{III} = 0.0048$ thus decrease considerably further.

In Fig. 8(c) the time function of the voltage components in phase a $u_{aI}(t) = Re\{\mathbf{u}_I\}$, $u_{aII}(t) = Re\{\mathbf{u}_{II}\}$ and $u_{aIII}(t) = Re\{\mathbf{u}_{III}\}$ are given as well as the phase voltage $u_a = u_{aI}(t) + u_{aII}(t) + u_{aIII}(t)$. The phase voltage u_a differs from u_{a0} phase end voltage only by zero voltage components.

The flux path of first coordinate system for $\hat{U}_1 = 0.9$ pu is drawn in Fig. 9. It is noticed that, the second vector has unusual direction: $-\pi/7$. This leads to grow of the loss factor up to $\Delta\Psi^2_I = 0.00071$ as it can be seen from Fig. 9(b), where the flux paths of all coordinate systems are given. At the same time the loss factor $\Delta\Psi^2_{II}$ considerably increases while $\Delta\Psi^2_{III}$ decreases in comparison with case $\hat{U}_1 = 0.95$.

For $\hat{U}_1 < 0.9$ $\Delta\Psi^2_{II}$ becomes higher than $\Delta\Psi^2_{III}$. In Fig. 10 the vector paths are drawn for $\hat{U}_1 = 0.88$ pu. The additional switching at $0 \leq \omega_1 t \leq \pi/14$ happens in phase f. $\Delta\Psi^2_{II}$ slightly decreases while $\Delta\Psi^2_I$ increases up to 0.0015. The the time function of the voltage components in phase a can be seen in Fig. 9(c).

If $\hat{U}_1 \leq 0.877$ pu the additional switching at $-\pi/14 \leq \omega t \leq \pi/14$ gradually passes from phase c and f to phase b and g (see Table II, α_1 and α_2 are given according to Fig. 5). In case of $\hat{U}_1 = 0.83$ pu the additional switching sequence at $0 \leq \omega_1 t \leq \pi/14$ happens two times in phase g. The space vector paths are shown in Fig. 11, where the flux of phase a together with its components is also given as $\Delta\Psi^2_a = \Delta\Psi^2_{aI} + \Delta\Psi^2_{aII} + \Delta\Psi^2_{aIII}$. Here $\Delta\Psi^2_{II}$ is 10 times greater than $\Delta\Psi^2_{III}$.

Finally the vector paths are given for $\hat{U}_1 = 0.8$ (see Fig. 12). In comparison with previous case it can be seen that $\Delta\Psi^2_{II}$ further increases while $\Delta\Psi^2_{III}$ decreases. Here

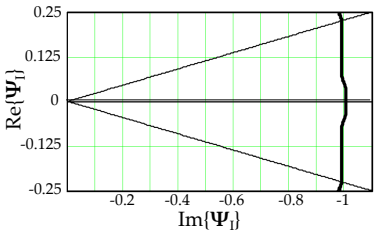

(a) Flux space vector path of I coordinate system, $-\pi/14 \geq \omega_1 t \geq \pi/14$

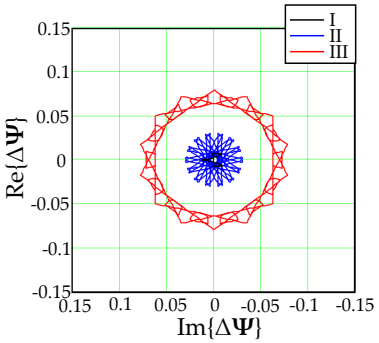

(b) Harmonic flux vector paths of coordinate systems I, II and III

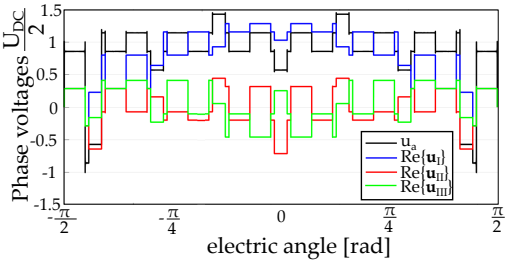

(c) Voltage components of phase a

Fig. 8. Additional switching, $\gamma = 5$, $U_1 = 0.95$ pu

$\Delta\Psi^2_I = 0.00045$ only.

The drawing vector paths give very important information on magnitude of stator and rotor harmonic losses and show which harmonic order produce those losses. This information is also important for an estimation of torque pulsation since they produce only by harmonics of the first coordinate system.

VI. Experimental Results

To verify the calculation results just described, laboratory measurements were carried out. The two-level seven-phase inverter were built by connecting parallel seven LMG5200 Gallium nitride half-bridge power stages. The inverter was

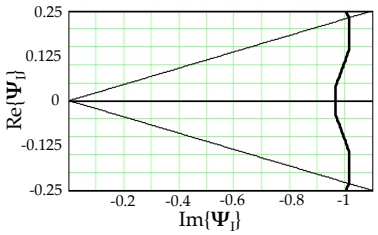

(a) Flux space vector path of I coordinate system, $-\pi/14 \geq \omega_1 t \geq \pi/14$

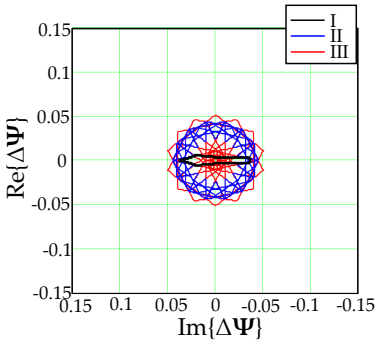

(b) Harmonic flux vector paths of coordinate systems I, II and III

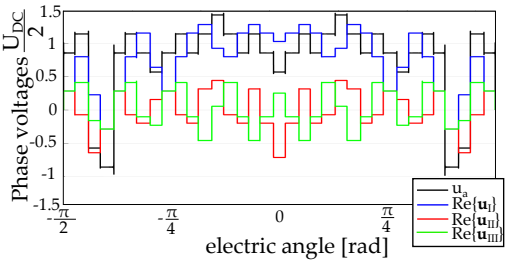

(c) Voltage components of phase a

Fig. 9. Additional switching, $\gamma = 5$, $U_1 = 0.9$ pu

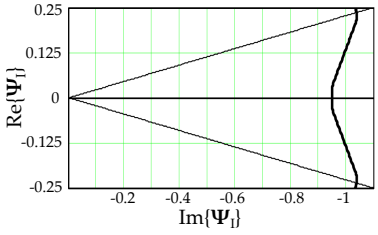

(a) Flux space vector path of I coordinate system, $-\pi/14 \geq \omega_1 t \geq \pi/14$

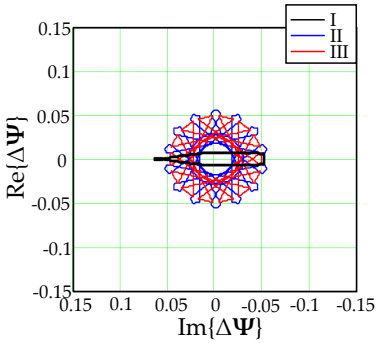

(b) Harmonic flux vector paths of coordinate systems I, II and III

Fig. 10. Additional switching, $\gamma = 5$, $U_1 = 0.88$ pu

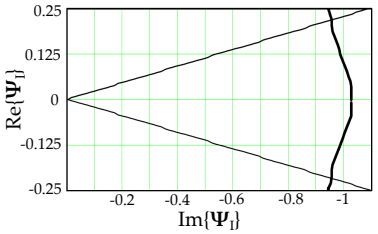

(a) Flux space vector path of I coordinate system, $-\pi/14 \geq \omega_1 t \geq \pi/14$

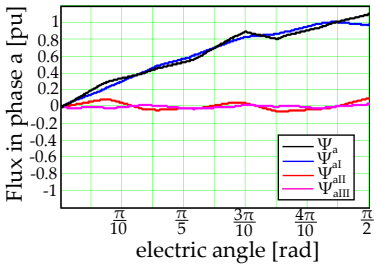

(b) Flux of phase and its components

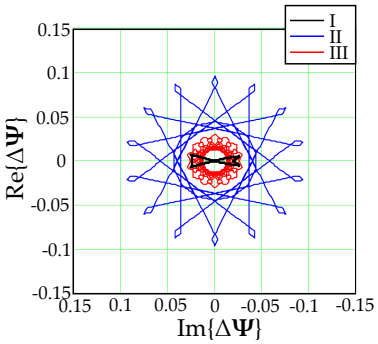

(c) Harmonic flux vector paths of coordinate systems I, II and III

Fig. 11. Additional switching, $\gamma = 5$, $U_1 = 0.83$ pu

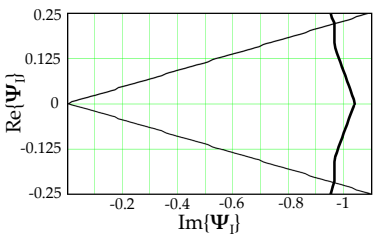

(a) Flux space vector path of I coordinate system

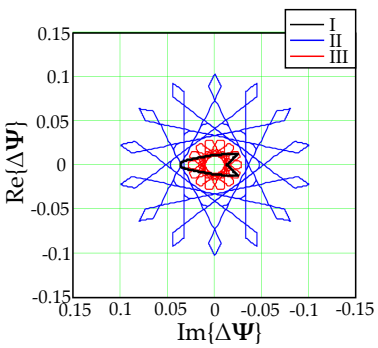

(b) Harmonic flux vector paths of coordinate systems I, II and III

Fig. 12. Additional switching, $\gamma = 5$, $U_1 = 0.8$ pu

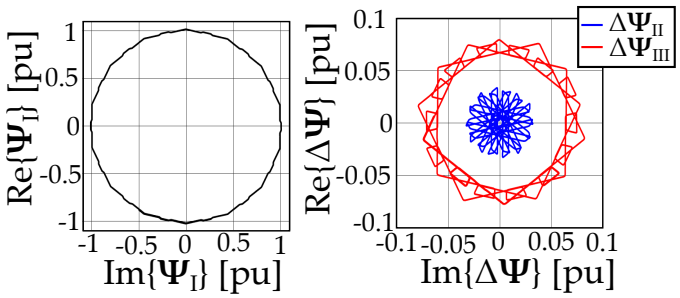

(a) Flux space vector path of I coordinate system and harmonic flux vector paths of coordinate systems II and III pu

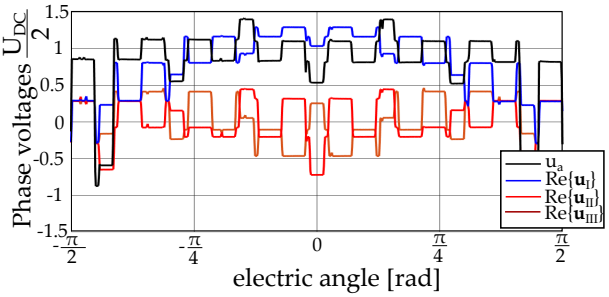

(b) Voltage components of phase a

Fig. 13. Experimental results, $\gamma = 5$, $U_1 = 0.95$ pu

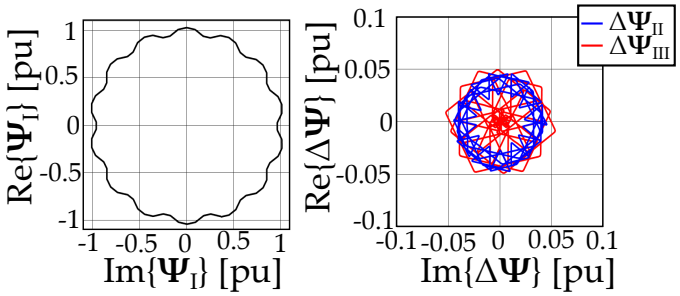

(a) Flux space vector path of I coordinate system and harmonic flux vector paths of coordinate systems II and III pu

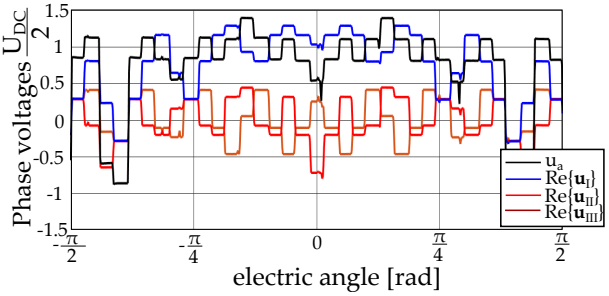

(b) Voltage components of phase a

Fig. 14. Experimental results, $\gamma = 5$, $U_1 = 0.9$ pu

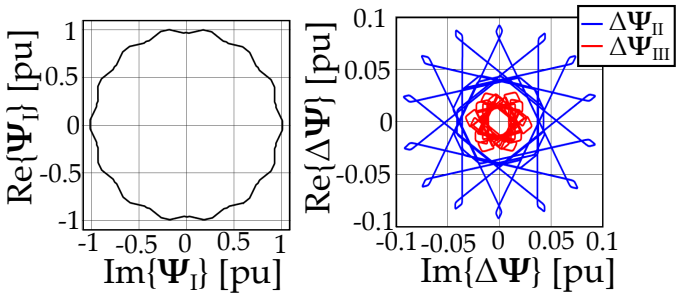

(a) Flux space vector path of I coordinate system and harmonic flux vector paths of coordinate systems II and III pu

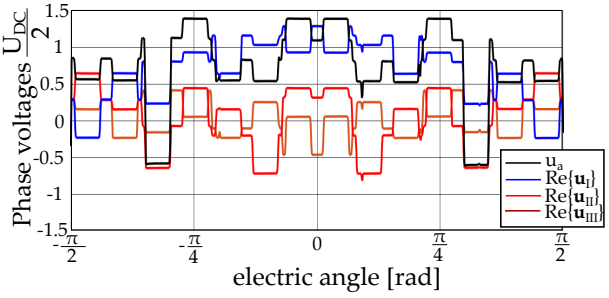

(b) Voltage components of phase a

Fig. 15. Experimental results, $\gamma = 5$, $U_1 = 0.83$ pu

loaded by an RL load. The PWM technique was implemented on a 32-bit DSP (TMS320F28379D). The DC link voltage was $U_{DC} = 50$ V and the output frequency is selected to be $f_1 = 100$ Hz for each working points. The flux signals are obtained by numerically integrating the measured output phase-end voltages.

Figure 13(a) presents the space vector path of fluxes in all coordinate systems at $U_1 = 0.95$ pu. The measured time function of the voltage components in phase a ($u_{aI}(t) = Re\{\mathbf{u}_I\}$, $u_{aII}(t) = Re\{\mathbf{u}_{II}\}$, $u_{aIII}(t) = Re\{\mathbf{u}_{III}\}$) as well as the phase voltage $u_a(t)$ are plotted on Fig. 13(b). As it can be seen in the figure, the measured phase voltage values in the different coordinate systems in the $0 \leq \omega_1 t \leq \pi/14$ region are the same as given in Table II.

Figure 14 and 15 present the same waveforms for $U_1 = 0.9$ pu and $U_1 = 0.83$ pu, respectively.

Comparing the measured waveforms with the calculated ones, it can be concluded that, the measured results are very similar to the calculated ones presented in the previous section. It can be concluded that, the laboratory tests verify the conclusions drawn in the previous section.

VII. Conclusions

Space vector investigation of multi-phase inverters in overmodulation region is given from viewpoint of ac motor harmonic losses. The decrease of seven phase motor harmonic losses is reached by additional inverter switching from $\gamma = 1$ (full control) to $\gamma = 5$ during time $\pi/7$ and additional switching angles are selected by minimizing of harmonic losses for a given fundamental voltage. The space vector investigation leads to an investigation of the different parts of overmodulation region in which different voltage vector rows are applied. The difficulty of investigation is explained by high number of voltage vectors. At same time the effectiveness in comparison with the investigation on basis of the phase and

line voltages in [9] - is not the best. One great advantage of space vector investigation should be mentioned: the space vector paths give good information on which harmonic groups create the stator and rotor harmonic losses. In comparison with three-phase machines especially the stator harmonic losses increase significantly, while the rotor harmonic losses of multi-phase machine are considerably lower.

REFERENCES

[1] M. Diana, R. Ruffo, and P. Guglielmi, "Pwm carrier displacement in multi-n-phase drives: An additional degree of freedom to reduce the dc-link stress," *Energies*, vol. 11, no. 2, 2018. [Online]. Available: https://www.mdpi.com/1996-1073/11/2/443

[2] P. Guglielmi, M. Diana, G. Piccoli, and V. Cirimele, "Multi-n-phase electric drives for traction applications," in *2014 IEEE International Electric Vehicle Conference (IEVC)*, Dec 2014, pp. 1–6.

[3] E. Levi, "Advances in converter control and innovative exploitation of additional degrees of freedom for multiphase machines," *IEEE Transactions on Industrial Electronics*, vol. 63, no. 1, pp. 433–448, Jan 2016.

[4] S. Halasz, "Pwm strategies of multi-phase inverters," in *2008 34th Annual Conference of IEEE Industrial Electronics*, Nov 2008, pp. 916–921.

[5] S. Halasz, "Continuous pwm strategies of multi-phase inverter-fed ac drives," *Periodica Polytechnica Electrical Engineering and Computer Science*, vol. 56, no. 2, pp. 51–62, 2012. [Online]. Available: https://pp.bme.hu/eecs/article/view/7161

[6] M. Ippisch and D. Gerling, "Analytic calculation of space vector modulation harmonic content for multiphase inverters with single frequency output," in *IECON 2019 - 45th Annual Conference of the IEEE Industrial Electronics Society*, vol. 1, Oct 2019, pp. 6187–6193.

[7] J. A. Riveros, J. Prieto, M. Rivera, S. Toledo, and R. Gregor, "A generalised multifrequency pwm strategy for dual three-phase voltage source converters," *Energies*, vol. 12, no. 7, 2019. [Online]. Available: https://www.mdpi.com/1996-1073/12/7/1398

[8] J. Prieto, F. Barrero, M. J. Durn, S. Toral Marn, and M. A. Perales, "Svm procedure for n-phase vsi with low harmonic distortion in the overmodulation region," *IEEE Transactions on Industrial Electronics*, vol. 61, no. 1, pp. 92–97, Jan 2014.

[9] S. Halasz, "Overmodulation region of multi-phase inverters," in *2008 13th International Power Electronics and Motion Control Conference*, Sep. 2008, pp. 682–689.

[10] E. Levi, R. Bojoi, F. Profumo, H. A. Toliyat, and S. Williamson, "Multiphase induction motor drives - a technology status review," *IET Electric Power Applications*, vol. 1, no. 4, pp. 489–516, July 2007.

[11] P. Stumpf and S. Halsz, "Optimization of pwm for the overmodulation region of two-level inverters," *IEEE Transactions on Industry Applications*, vol. 54, no. 4, pp. 3393–3404, July 2018.

[12] S. Halasz, "Discontinuous modulation of multiphase inverter-fed ac motors," in *2009 13th European Conference on Power Electronics and Applications*, 2009, pp. 1–9.

[13] S. Halasz, "Space vector investigation of multi-phase inverter-fed ac drives in overmodulation region," in *Power Electronics for Industrial and Renewable Energy Convrsion Conference, Doha, Qatar*, 2011, pp. 69–74.